Computers in Biology and Medicine 112 (2019) 103379

Contents lists available at ScienceDirect

Computers in Biology and Medicine

journal homepage: www.elsevier.com/locate/compbiomed

Empirical mode decomposition based ECG features in classifying and tracking ventricular arrhythmias

M. Hotradat[a], K. Balasundaram[a], S. Masse[b], K. Nair[b], K. Nanthakumar[b], K. Umapathy[a,*]

[a] Department of ECBE, Ryerson University, 350 Victoria St., Toronto, M5B2K3, Canada
[b] THFCFML, Toronto General Hospital, 200 Elizabeth St., Toronto, M5G2C4, Canada

ARTICLE INFO

Keywords:
Dynamic features
Empirical mode decomposition
Pattern classification
Ventricular fibrillation
Ventricular tachycardia

ABSTRACT

Ventricular arrhythmias (VA) are life-threatening pathophysiological conditions that seriously impact the normal functioning of the heart. Ventricular tachycardia (VT) and ventricular fibrillation (VF) are the two well known types of VA. VF is the lethal of the VAs and could be characterized by its organizational progression over time. The success of cardiac resuscitation strongly depends on the type of VA, its evolution over time and response to therapy. Due to the time critical nature of VF, computationally efficient quantification of VAs and swift feedback are essential. This work attempted to arrive at computationally efficient and data-driven techniques based on Empirical Mode Decomposition for classifying and tracking VAs over time. The approaches are divided into two aims: (1) 'in-hospital' scenarios for characterizing the dynamics of VA episodes to assist clinicians in planning long-term therapy options, and (2) 'out-of-hospital' scenarios for providing near real-time feedback to detect/track the progression of VAs over time to assist medical personnel select/modify therapy options. Using an ECG database of 61 60-s VA segments obtained for classifying VT vs. VF and sub-classifying VF into organized VF (OVF) and disorganized VF (DVF), maximum classification accuracies of 96.7% (AUC = 0.993) and 87.2% (AUC = 0.968) were obtained for classifying VT vs. VF and OVF vs. DVF during 'in-hospital' analysis. Additionally, two near real-time approaches were presented for 'out-of-hospital' analysis where average accuracies of 71% and 73% were achieved for VT/VF and OVF/DVF classification, as well as demonstrating strong potential for monitoring VA progressions over time.

1. Introduction

Ventricular arrhythmias (VA) are life-threatening pathophysiological conditions that seriously impact the normal functioning of the heart. Ventricular tachycardia (VT) and ventricular fibrillation (VF) are the two well known types of VA. VT is characterized by unusually fast ventricular contractions, resulting in a drastic decrease in circulation due to the reduction in blood filling the ventricles [1]. VT will often devolve into VF over time, which is the most lethal type of VA. During VF the ventricles of the heart fail to contract in an organized manner at all, resulting in an almost complete loss of circulation to vital organs. If this condition persists for few minutes without medical treatment it becomes fatal. Annually in North America, 350,000 people die from sudden cardiac death (SCD) [2], many of those cases are related to VF. Most of these SCDs occur in the 'out-of-hospital' VF incidences. In spite of decades of research, there is no fool proof treatment option for VF and despite the technological advances, survival from 'out-of-hospital' cardiac arrest remains extremely low [3]. One study based on Resuscitation Outcomes Consortium registry including 7 US and 3 Canadian sites (with 96662 out-of-hospital cardiac arrest) reports the survival to discharge to be less than 10% [3].

In order to improve the current treatment options, there are many ongoing research efforts that are attempting to understand, characterize, and quantity VAs to obtain meaningful markers on its evolution and response to therapy. There are also strong indications that in near future treating VF via focal ablations will be a potential possibility for 'in-hospital' VF or symptomatic patients suffering VF [4,5]. Krummen et al. demonstrated that VF is perpetuated by a finite number of stable rotors, and targeting these specific sites with focal ablation therapy can significantly reduce VF inducibility [4,6,7]. Ho et al. also demonstrated that focal ablation therapy prevented inducibility of VF by targeting rotor sites [5]. Recent past studies supporting rotor theory have demonstrated spatio-temporal organization during VF [8–11]. Rotor theory is one of the 2 well-known theories on the mechanism behind VF, the other being the multiple-wavelet theory [12]. In the rotor theory, VF is initiated and maintained by organized rotating

* Corresponding author.
E-mail address: karthi@ee.ryerson.ca (K. Umapathy).

https://doi.org/10.1016/j.compbiomed.2019.103379
Received 11 April 2019; Received in revised form 10 July 2019; Accepted 1 August 2019

sources called rotors [13]. As per this theory and many existing works supporting this theory, the difference between an organized VF and disorganized VF is explained by the number of rotors and their characteristics (i.e. meandering, stable, transient etc). While many of the existing studies have shown the organizational aspects spatio-temporally, temporal organization has also been indirectly quantified by many existing methods using surface ECGs [14,15]. In addition, the time from VF onset (or whether it is early VF or late VF) is widely believed to influence the organization. Some treatment options like Cardio Pulmonary Resuscitation (CPR) and anti-arrhythmic drugs have also been shown to influence the organization of VF and/or rotor characteristics [16,17]. All of the above evidences support that during the temporal evolution of VF, VF undergoes many stages with varying organization and the time-varying organizational aspects of VF may hold clues on the conducive state of the heart to receive therapy (such as CPR, anti-arrhythmic drugs, shock, or focal ablation) and to monitor the response to the therapy. In other words, quantifying the temporally evolving organizational aspects of VF could significantly assist clinical community in planning appropriate 'out-of-hospital' or 'in-hospital' treatment options for VF. One such attempt to quantify the organizational aspects is to sub-categorize VF into temporally organized VF (OVF) and disorganized VF (DVF) [18] using ECG features. This sub-categorization is based on subtle variations in the temporal complexity of these two conditions. Classifying OVF and DVF is a challenging problem due to the natural overlap between them, and has been attempted in the past with fair success [18,19].

There have been works in the past extracting 'static' features from VF to quantify its organization over fixed windows. While effective for some applications, these measures are unable to capture the dynamic temporal evolution of VF, a crucial element for its characterization. To capture the time-varying characteristics of VAs, some works have aptly used instantaneous time-frequency (TF) features [20–24]. However, due to the high computational complexity of extracting these TF derivatives, they have been prohibitive for real-time feedback of VF. Through the use of computationally efficient empirical mode decomposition (EMD) [25] and Hilbert Spectrum (HS) [26], our work attempts to bridge the gap that has been inhibiting the use of instantaneous TF and dynamic features for near real-time feedback of VAs, especially in 'out-of-hospital' VF incidences. In our preliminary work using a smaller electrocardiogram (ECG) database and smaller feature set, instantaneous TF features were extracted from the EMD derived HS in order to classify VT, OVF, and DVF [27]. While this approach proved effective for classifying these VAs for long-term scenarios, it did not address the problem of assisting Emergency Medical Services (EMS) in accurately assessing VAs for 'out-of-hospital' settings where ECG data is being acquired in real-time. It may also be useful to track the changes occurring in the VAs over time so that overall trends within VAs may be detected. Analyzing these VA trends in real-time may provide valuable feedback to assist with field therapy adjustments, which may improve patient outcomes.

In this work, we will present approaches that are applicable for 'in-hospital' settings (long-term), improving upon our preliminary work [27], as well as novel approaches for 'out-of-hospital' settings (short-term) which aim to provide near real-time feedback to assist medical personnel in detecting VAs and tracking their progression over time. Using EMD derived HS and EMD, instantaneous TF features as well as windowed energy-based features will be extracted to help discriminate between 3 types of VAs. A block diagram outlining the performed study is shown in Fig. 1. The paper is organized as follows. Details of database and pre-processing are provided under Section 2. Methods in Section 3 present details on EMD based feature extraction, pattern classification, and VA trend analysis. Results for the different proposed approaches are provided in Section 4. Discussion and conclusions are provided in Section 5 and Section 6 respectively.

2. Database & pre-processing

The ECG database used in this study was extracted from open source MIT-BIH VA database and the Creighton University VT database [28]. The database consisted of 61 continuous 60-s ECG VA segments including: 22 (mostly) VT, 17 (mostly) OVF and 22 (mostly) DVF. These segments were extracted from 22 different patients. Considering that VF is highly non-stationary in nature, VA segments extracted from the same patient recording but at different times may be treated as independent records. Some of the 4-s VF segments from the work of Balasundaram et al. [18] were included within the 60-s VF segments of this database. The ground truth label for the three types of VAs were provided by our clinical collaborators from Toronto General Hospital. Due to natural variations in the VA segments over 60-s duration, they were labeled as 'mostly' VT or VF based on what the majority of each segment was. The use of longer duration 60-s segments was predicated on the desire to capture those natural variations present in the VAs which evolve over time, mimicking real-world scenarios and capturing dynamic VA trends. This is unlike previous works which only attempted to quantify VAs over shorter windows. The 60-s VA segments were sampled at 250 Hz (15000 samples), and a bandpass filter with a lower cutoff of 0.3 Hz and upper cutoff of 30 Hz was used to retain the frequency band of interest [18,29]. The VA segments were also normalized to the same cumulative energy in order to remove any potential bias caused by the absolute amplitude of the signals. Fig. 2 shows 3 samples of VT, OVF and DVF segments from this database, zoomed in on a 10-s portion of the total 60-s length.

For the 'out-of-hospital' (short-term) approach, EMD was performed on 4-s segments of the total 60-s ECG signals. The ECG signals were segmented in order to simulate the real-time acquisition of data in emergency settings. A buffer of 4-s was necessary to allow adequate information to be available for feature extraction. For the 'in-hospital' (long-term) approach of this work however, the entire 60-s duration of the ECG segments was utilized at once to maximize the amount of information available to make classification decisions in offline settings.

3. Methodology

The methodology that was used to perform this study will be explained below. Firstly, the method of EMD will be explained and how it was implemented. Subsequently, the construction of the HS will be explained, followed by the feature extraction of non-instantaneous energy-based features and instantaneous TF features from the HS. Then, the pattern classification techniques that were used to discriminate between the 3 VA groups will be discussed, and lastly the VA scoring method used in the VA trend analysis will be explained.

3.1. Empirical mode decomposition

Introduced by Huang et al. [25], EMD is a data-driven and adaptive data decomposition technique. Instead of relying on a basis function, it decomposes the data based on its intrinsic properties. It has the ability to decompose any given signal into intrinsic mode functions (IMF). The underlying oscillatory modes within the data are represented by these IMFs. EMD has a low computational complexity similar to the Fast-Fourier-Transform, with a big 'O' notation of $O(NlogN)$ [30]. This makes it a suitable technique for this proposed work utilizing real-time features. The two conditions an IMF must satisfy are: (1) the number of minima and maxima must be equal or differ by one at most, and (2) the average envelope designated by the local extrema (minima and maxima) must have a mean value of zero. The EMD sifting algorithm is briefly described below using a discrete-time signal $x[n]$ (readers are referred to Refs. [25,31] for the detailed step-by-step process):

The local minima and maxima of $x[n]$ are identified and connected to construct the lower envelope E_L and the upper envelope E_U, respectively. The mean envelope, E_μ, is computed according to the

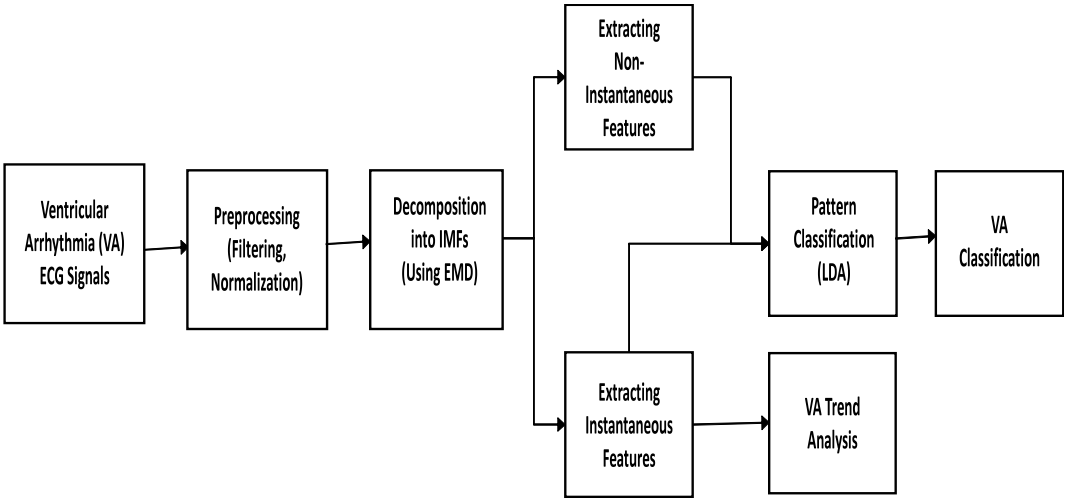

Fig. 1. The block diagram outlining the performed study.

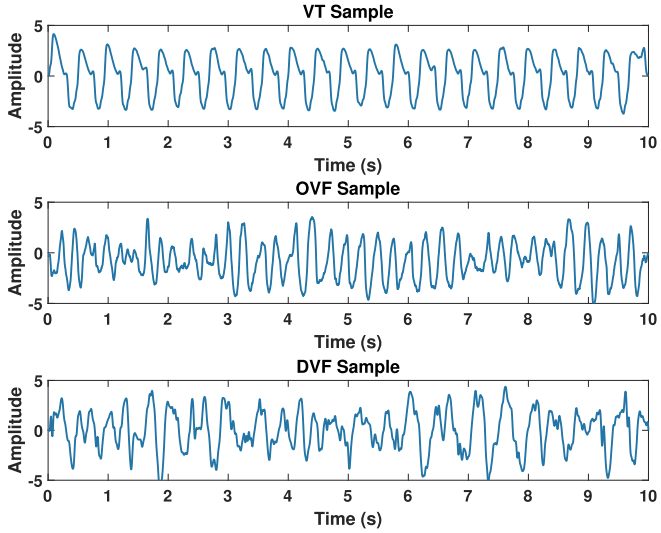

Fig. 2. VT, OVF, and DVF samples from the proposed database, zoomed in on a 10-s portion for better visual illustration of signal characteristics.

formula: $E_\mu = (E_U + E_L)/2$ and subtracted from $x[n]$ to obtain the updated $x[n]$. The steps above are continued until $x[n]$ fulfills necessary IMF conditions (see above). Upon completion, $x[n]$ is designated as $c_1[n]$, the first IMF. The first residual, $r_1[n]$, is obtained by subtracting $c_1[n]$ from the original $x[n]$. The $r_1[n]$ is now designated as the new initial point. The above steps are repeated until every possible IMF $c_i[n]$ is decomposed leaving the final residue, $r_J[n]$.

To reconstruct $x[n]$, the J IMFs are summed with the final residue, $r_J[n]$:

$$x[n] = \sum_{i=1}^{J} c_i[n] + r_J[n] \tag{1}$$

The decomposed IMFs may reveal valuable information regarding the underlying structures that compose different VAs. In this work, the upper and lower envelope construction was done using the piecewise cubic Hermite interpolating polynomial (PCHIP) approach [32], since it was shown to reduce overshooting in biomedical signals and have a reduced computational complexity compared to the alternative cubic spline method. There were a number of decomposition criteria used to control the number of IMFs. These criteria were: 'relative sifting tolerance' (0.2) [25], which ensured that successive IMFs retained enough physical meaning in their amplitude/frequency modulations, the maximum number of sifting iterations (100), the minimum number of extrema present within an IMF (1), and the 'maximum energy ratio' [33], which halted EMD once the energy of the final residual fell below 1% of the original signal.

3.1.1. Selection of IMFs

For 'out-of-hospital' analysis, the decomposed IMFs from each 4-s segment were organized according to descending cumulative energy, and only the top 3 IMFs were used. This was done since the majority of the segment's energy was concentrated there, and in order to keep the comparison uniform between each segment. Due to the computational efficiency of the implementation of EMD, this approach would lend well to near real-time applications. From the top 3 IMFs, the HS was constructed and feature extraction was performed.

For 'in-hospital' analysis, the total number of IMFs decomposed from each 60-s ECG signal ranged between 7 and 9. Since the segments were longer and thus more complex, more IMFs were decomposed compared to the 'out-of-hospital' approach. The extracted IMFs were sorted based on descending energy, and the top 7 IMFs were used in further analysis. This was again done in order to keep the comparison between different ECG segments as consistent as possible. Since the majority of the signals' energy was concentrated in those 7 IMFs (>90%), minimal signal information was discarded. The IMFs were used in construction of the HS and feature extraction.

3.2. Hilbert energy spectrum

The decomposed IMFs were used to facilitate TF analysis through the HS. EMD used along with the HS is also called the Hilbert-Huang Transform [26]. The HS, a time-frequency representation (TFR), reveals how the energy of a signal is changing relative to both time and frequency. Before constructing the HS, the Hilbert transform was first used to convert the IMFs, $c_i[n]$, into their analytic form, $z_i[n]$. The HS is defined by the following equations [26,34]:

$$HS_i(\omega, n) = \begin{cases} a_i^2(n), & \omega = \omega_i(n) \\ 0, & otherwise \end{cases} \tag{2}$$

$$HS(\omega, n) = \sum_{i=1}^{k} HS_i(\omega, n) \tag{3}$$

Where $a_i(n)$ and $\omega_i(n)$ are the instantaneous amplitude and instantaneous frequency of the i^{th} analytic IMF, $z_i[n]$, respectively. An important note is that the instantaneous amplitude $a_i^2(n)$ is squared in the above equation, which makes it an energy spectrum as opposed to an amplitude spectrum [26]. Compared to other TFRs like the Wigner-

Ville Distribution, the HS has a number of benefits. These benefits include better TF resolution [26], no cross-term interference, and lower computational cost through the use of EMD. From the TF plane of HS, instantaneous TF features can be extracted. These instantaneous features can be used to quantify the dynamic behaviour seen in VAs over time.

3.3. Feature extraction

In this section, the feature extraction will be explored. Firstly, the energy-based features extracted from the IMFs will be discussed. Following that, the instantaneous TF features extracted from the HS will be explained.

3.3.1. IMF energy-based features

From the set of decomposed IMFs, two energy-based features were initially extracted. The first of those was the energy ratio variance (ERV). ERV was computed by evaluating the variance of the normalized energy ratios from the set of IMFs as given below [27]:

$$ERV = \frac{1}{m-1}\sum_{j=1}^{m}(E_j - \bar{E})^2 \tag{4}$$

Where E_j is the energy ratio of the j^{th} IMF, and $\bar{E}$ is the mean of the normalized energies. A signal's organizational complexity may be measured by the ERV. For example, a more mono-component signal will have the majority of its energy content focused around a single IMF resulting in a higher ERV, while a more multi-component signal will have its energy more uniformly distributed around all IMFs resulting in a lower ERV.

The second energy based feature that was extracted similar to ERV was the energy ratio skew (ERS). The ERS is computed by calculating the skewness measure of the normalized energy ratios of the IMFs. The energy ratios are treated as points in a probability distribution, and ERS is computed by the following equation [35]:

$$ERS = \frac{1}{m}\sum_{j=1}^{m}\frac{(E_j - \bar{E})^3}{\sigma^3} \tag{5}$$

In Equation (5), σ^3 is the cubed standard deviation of the normalized energy ratios. The ERS quantifies the distance that the energy ratios are deviated from the mean value. A skew below the mean will be negative, and a skew above the mean will be positive. This feature also helped to measure the amount of complexity in the signal by quantifying the amount of variability in the energy distribution of the IMFs.

For the 'out-of-hospital' approach, the ERV and ERS features were extracted for every 4-s ECG segment. Additionally, a cumulative averaging strategy was implemented, where every subsequent value of ERV/ERS was averaged with the previous value. Doing so enabled the observation of relative dynamic changes between consecutive 4-s segments of the VA signals. The formula for computing the cumulative average of ERV is shown below:

$$ERV(m) = \frac{ERV(m) + ERV(m-1)}{2} \tag{6}$$

Where $ERV(m)$ is the current ERV value, and $ERV(m-1)$ is the previous ERV value. Likewise, the same formula was used for computing ERS values.

In the 'in-hospital' approach, to use ERV and ERS to monitor dynamic VA changes over time, these features were computed over sliding windowed segments of all IMFs resulting in one value per window. Two different window sizes were chosen, which were 1-s (250 samples) and 4-s (1000 samples). These window sizes were selected in order to capture the rapid changes occurring in the VAs, as well as the slower VA fluctuations over time. Fig. 3 shows the 1-s windowed ERV values for samples of the 3 VA groups. It was seen that the ERV values were highest for the VT sample, lower for the OVF sample, and the lowest for the DVF sample. Thus, quantifying these observed differences over time may aid in classifying these VA groups.

3.3.2. Instantaneous features

From the constructed HS, the following instantaneous TF features were extracted: instantaneous mean frequency (IF) and squared instantaneous bandwidth (IB^2) [27,36,37]. The IF and IB^2 provide instantaneous tracking of a signal's spectral changes over time. The IF can be expressed as below [24,38]:

$$IF(n) = \frac{\sum_{\omega}\omega HS(\omega, n)}{\sum_{\omega} HS(\omega, n)} \tag{7}$$

As well, the IB^2 can be expressed as below [36,37,39]:

$$IB^2(n) = \frac{\sum_{\omega}\omega^2 HS(\omega, n)}{\sum_{\omega} HS(\omega, n)} - IF(n)^2 \tag{8}$$

$IF(n)$ may be conceptualized as the average frequency at every time point, n, while $IB^2(n)$ quantifies the spectral spread at every time point, n.

Additionally, in order to better appreciate the changes observed in the IF and IB^2 over time, the gradient for each of them was also computed. This would magnify any rapid changes, and make it more quantifiable. The gradient was computed using the central difference according to the following equation [40]:

$$Gradient_{IF}(j) = \frac{1}{2}(IF(j+1) - IF(j-1)) \tag{9}$$

Where $IF(j)$ is the j^{th} time sample in $IF(n)$. This is repeated for every value of IF. The edge values of 1 and N were computed by single-sided differences. This formula was applied identically to calculate the gradient of IB^2. The IF and IB^2 were low-pass filtered (10-Hz) prior to the gradient computation to remove high frequency artifacts, so that a smoother representation of the general changes occurring in the instantaneous derivatives over time may be seen.

Another instantaneous feature that was obtained independently from the HS was the instantaneous energy (IE). The fundamental way to calculate the IE from a time-domain signal is to take the squared magnitude of the signal of interest [41]. For this work however, it was calculated using the sum of the top 2 highest energy IMFs decomposed from each filtered and normalized ECG segment. Due to its construction, the IE will hereby be denoted as IE_{12}, and it was calculated as:

$$IE_{12}(n) = \sum_{i=1}^{2}|z_i(n)|^2 \tag{10}$$

Where $z_i(n)$ is analytic form of the i^{th} IMF, sorted from highest to lowest energy. The IE_{12} will indicate how the energy of the dominant components of the signal are dynamically changing over time. Combinations of various IMFs were experimented with, but the best results for discriminating between the VA groups was obtained by using the top 2 IMFs for IE_{12}. The majority of the signal's energy is concentrated within those top 2 IMFs.

The three extracted instantaneous features will allow for the observation of dynamic changes occurring in the VAs over time. This insight into the temporally evolving nature of the VAs may prove useful in discriminating them. In order to quantify the dynamic changes seen in the windowed energy-based and instantaneous features, statistical measures were computed.

3.3.3. Statistical measures

In order to quantify the dynamic behaviour of the instantaneous and windowed features extracted above, a number of statistical measures were calculated. These measures will help to highlight differences between the 3 VA groups so that they can be discriminated effectively. From the windowed ERV/ERS features, the following statistical measures were calculated: mean, median, variance, RMS-value, and slope.

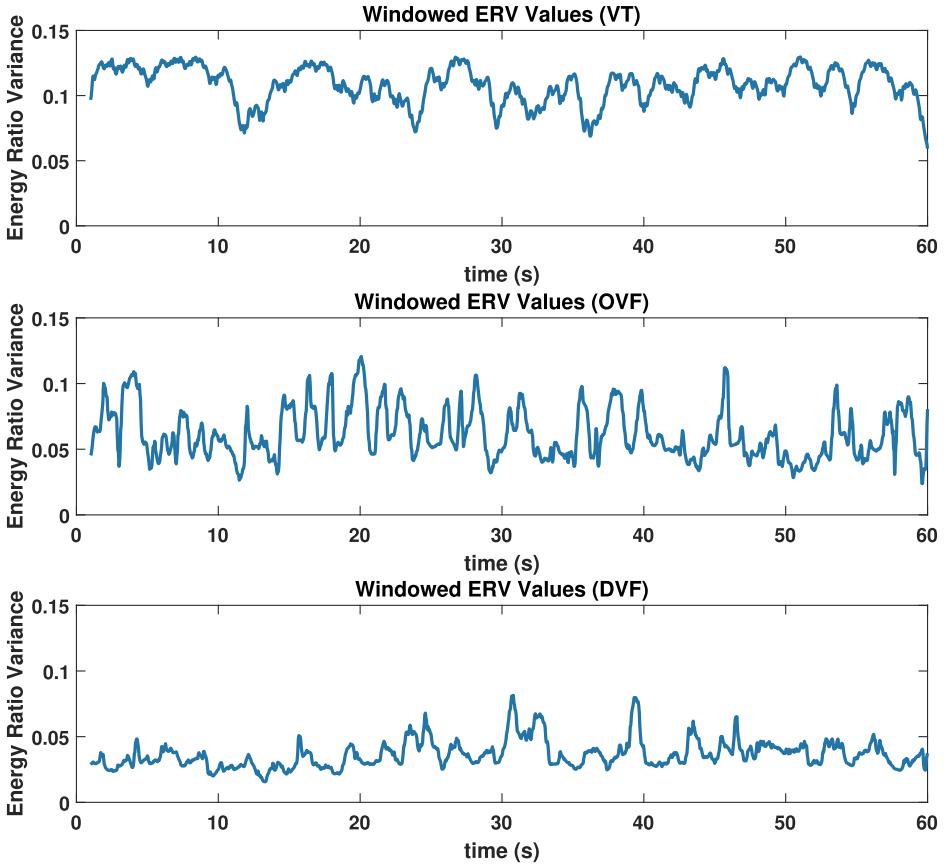

Fig. 3. The sliding (1-s) windowed ERV values for a sample VT, OVF, and DVF signal.

These same statistical measures were also computed from the three instantaneous features. Additionally, from the gradient IF and IB^2, the mean and median were computed to capture their overall behaviour over time.

3.4. Pattern classification

A two stage binary pattern classifier was trained using the above extracted statistical measures to differentiate the 3 VA groups. In the first stage VT and VF were classified, and in the second stage the rightly identified VF were further divided into OVF and DVF. A linear classifier based on linear discriminant analysis (LDA) was used with leave-one-out cross-validation (LOOCV) [42]. The statistical software package IBM SPSS 25.0 was used to perform the analysis [43]. A LDA based classifier was chosen so that the emphasis was placed on the discriminatory power of the features used to train the classifier. Also, since LDA is a linear classifier, it is less susceptible to overfitting than more complex classifiers. A few recent biomedical applications which utilized LDA based classifiers are in brain computer interfacing for classifying electroencephalogram signals [44], in pattern recognition of electromyography signals for controlling wearable exoskeletons [45], as well as in a review paper some recent ECG classification works were highlighted by Berkaya et al. [46]. LOOCV is the extreme form of cross-validation with least bias, and it is the preferred method for small, biomedical signal databases. It removes the possibility of selection bias when designating the training and testing sets.

In order to calculate the classification accuracy, the following equation was used:

$$Accuracy = \frac{TP + TN}{TP + FP + TN + FN} \tag{11}$$

Where TP is True Positive, TN is True Negative, FP is False Positive, and FN is False Negative.

3.5. VA trend scoring algorithm

In order to use the instantaneous features for tracking the dynamics of VAs over time for real-world applications, a trend analysis approach was developed. Inspired by time-trend analyses from other fields (i.e. financial) [47], this approach was designed in order to monitor instantaneous changes occurring in VAs and provide feedback on its temporal progression. The algorithm was as follows:

- Using the full 60-s ECG VA segments, IF, IB^2 and IE_{12} were extracted, and the median values for each feature were computed. For each of the 3 VA groups (VT, OVF, DVF) the mean of those median values were calculated. Those resulting values were used to create thresholds to separate the different VA groups.
- Each of the 60-s ECG VA segments were windowed in order to simulate the trend analysis in near real-time. Initially a 4-s segment of the ECG signal was analyzed, where the EMD-HS was constructed and the 3 instantaneous features were extracted. Subsequently, the sliding window was expanded by 100 samples (0.4s) each time and the HS was updated along with the instantaneous features. This was continued until the entire 60-s ECG segment was analyzed.
- Each of the windowed segments were scored by computing the median values of the 3 instantaneous features and comparing them to the previously defined thresholds. The logic rules used to score the VA segments were based on previous literature about the spectral and temporal behaviour of these VAs. The rules for scoring the segments is described below:
  1. If the median (IF, IB^2) of the segment was ≤ the mid-point between the VT and OVF thresholds ((VT_{th} + OVF_{th})/2), then score it as VT (0).

2. If the median (IF, IB^2) of the segment was > $((VT_{th} + OVF_{th})/2)$, but ≤ the mid-point between the OVF and DVF thresholds $((OVF_{th} + DVF_{th})/2)$, then score it as OVF (1).
3. Otherwise, score the segment was DVF (2).

The scoring rules were similar for IE_{12}, only opposite in that VT was expected to have the highest median energy and DVF the lowest median energy. Each windowed segment received one score from each of the 3 instantaneous features. From those 3 scores, the modal score was identified and selected as the overall score for that segment.

- Lastly, a cumulative averaging strategy was implemented to help capture the dynamic changes between the windowed VA segments over time. For all subsequent segments after the initial segment, the previous segment's score was averaged with the current segment's score to produce the next segment's score. The equation for computing the cumulative average score was:

$$Score(m) = \frac{Score_{mode}(m) + Score(m-1)}{2} \quad (12)$$

Where $Score_{mode}(m)$ represents the modal score generated from the 3 instantaneous features for the current m^{th} windowed segment, and $Score(m-1)$ is the score from the previous segment.

Calculating the cumulative scores over the entire 60-s duration of the ECG segments created a visual trend of how the VA is evolving over time, providing near real-time feedback to the user on its progression.

4. Results

The results presented will be divided into 3 sub-sections. The first sub-section will discuss the results for short-term VA classification, appropriate for 'out-of-hospital' emergency aid. The second sub-section will show the results of the long-term VA classification, appropriate for 'in-hospital' analysis. The last sub-section will explore the results of VA Trend Analysis, where dynamic changes in VAs over time were monitored to track their progression for 'out-of-hospital' scenarios.

4.1. Out-of-hospital (short-term) VA classification

In this approach, the VA signals were analyzed on 4-s segments at a time. By doing so, this method would allow the user to obtain a VA classification result as swiftly as 4-s. The user may receive near real-time classification feedback on a patient's VA as frequently as desired. In order to verify the robustness of this technique, it was tested on 3 different time durations: 20-s, 40-s, and 60-s. This enabled for the assessment of the performance of this approach while simulating the acquisition of patient data in real-world scenarios. Only the windowed ERV/ERS statistical features were used in this part of the study.

For each trial, the combination of features that produced the highest classification accuracy was used to train each classifier. In the 20-s trial, the classification accuracy achieved for the VT vs. VF classification was 63%. In the OVF vs. DVF classification, a cross-validated accuracy of 72% was obtained. In the 40-s trial, the VT vs. VF classification accuracy achieved was 79%. For the subsequent OVF vs. DVF classification, an accuracy of 67% was achieved. Lastly in the 60-s duration trial, the best result for VT vs. VF was 72% accuracy, and in the OVF vs. DVF classification an overall accuracy of 81% was obtained. A summary of the features used is shown in the left 2 columns of the below Table 1. The ERV feature denoted by the sub-name 'final' was the final cumulative average value of ERV obtained over the course of the monitoring duration.

A combination of these features provided the best classification results reported for the 20-s, 40-s, and 60-s trials. The boxplots showing the difference in the distribution of the feature values is provided in Fig. 4. The top row shows the features used for VT vs VF classification and the bottom row shows the features used for OVF vs DVF classification.

Table 1
Summary of features used for both **Short-Term** and **Long-Term** VA classification.

Short-Term Features		Long-Term Features	
VT vs. VF	OVF vs. DVF	VT vs. VF	OVF vs. DVF
ERS median	ERS mean	grad. IF median	IB^2 slope
ERV final	ERS var.	IE_{12} median	grad. IF median
ERS mean	ERV mean	IE_{12} var.	IE_{12} mean
ERV var.	ERV median	ERS var. (1s)	ERS total
	ERS median	ERV slope (4s)	ERV var. (4s)
	ERS RMS		

4.1.1. Comparative analysis

In order to validate the above results, 3 features previously used in literature for classifying VAs were also tested. The features used were: dominant frequency (DF), temporal entropy (EN), and spectral entropy (SE). These features were extracted from the same database over 1-s and 4-s sliding windows identical to how ERV and ERS were captured. They were used to train the LDA-based classifier and tested on the same 3 duration trials. In the 20-s trial, the accuracy achieved for the first stage (VT vs. VF) was 83%. In the second stage (OVF vs. DVF), the classification accuracy achieved was 64%. In the 40-s duration trial, the total classification accuracy for the first stage was 88%, and in the second stage the classification of 60% was obtained. Finally in the 60-s trial, the total cross-validated accuracy for the first stage was 90%, and in the second stage the total classification accuracy obtained was 76%.

4.2. In-hospital (long-term) VA classification

In the initial classification stage (VT vs VF), 22 VT segments and 39 VF (OVF and DVF) segments were there in total. The best classification accuracy was obtained when training the classifier with the combination of the following 5 features: IE_{12} variance, IE_{12} median, gradient IF median, ERV slope (4s) and ERS variance (1s). A summary of the features used for the long-term VT vs. VF classification stage is shown in the 3rd column of Table 1. The top row of Fig. 5 shows the boxplots of the features used for VT vs. VF classification.

From the top row of Fig. 5, it is evident that IE_{12} variance and IE_{12} median are the top 2 dominant features. It can be clearly seen that the IE_{12} median is greater for VT than the VF. This showed that the amount of energy over time is generally higher for VT than VF. Because VF is a worsened condition than VT, this may be resulting in a lower amplitude in the ECG recording. On the other hand, IE_{12} variance was higher for VF than VT. Due to the increased disorganization within VF, greater amplitude and energy variations were present compared to VT. This resulted in the variability of the energy to be higher for the VF group. Overall, the energy content over time combined with the other three features proved to be useful for separating the VT and VF groups.

The total classification accuracy achieved was 96.7%. If we assume that VF is the positive class and VT is the negative class based on relative severity, the sensitivity was 100% and the specificity was 90.9% for this stage. Table 2 shows the summarized results below. Overall, 2 out of the 22 VT segments were mis-classified, but none of the VF segments were mis-classified. The area under the curve (AUC) for the receiver operating characteristic (ROC) curve of this classifier was equal to 0.993, validating the strong discriminating power. The p-value of the linear discriminant scores (i.e. weighted sum of feature values used for classification) was also significant ($p < 0.01$).

In the second stage of classification where OVF was classified from DVF, there were 17 OVF and 22 DVF segments used. The highest classification accuracy was achieved with the following five features: IB^2 slope, gradient IF median, IE_{12} mean, ERS total, and ERV variance (4s). A summary of the features used for the long-term OVF vs DVF classification stage is shown in the 4th column of Table 1. The ERS

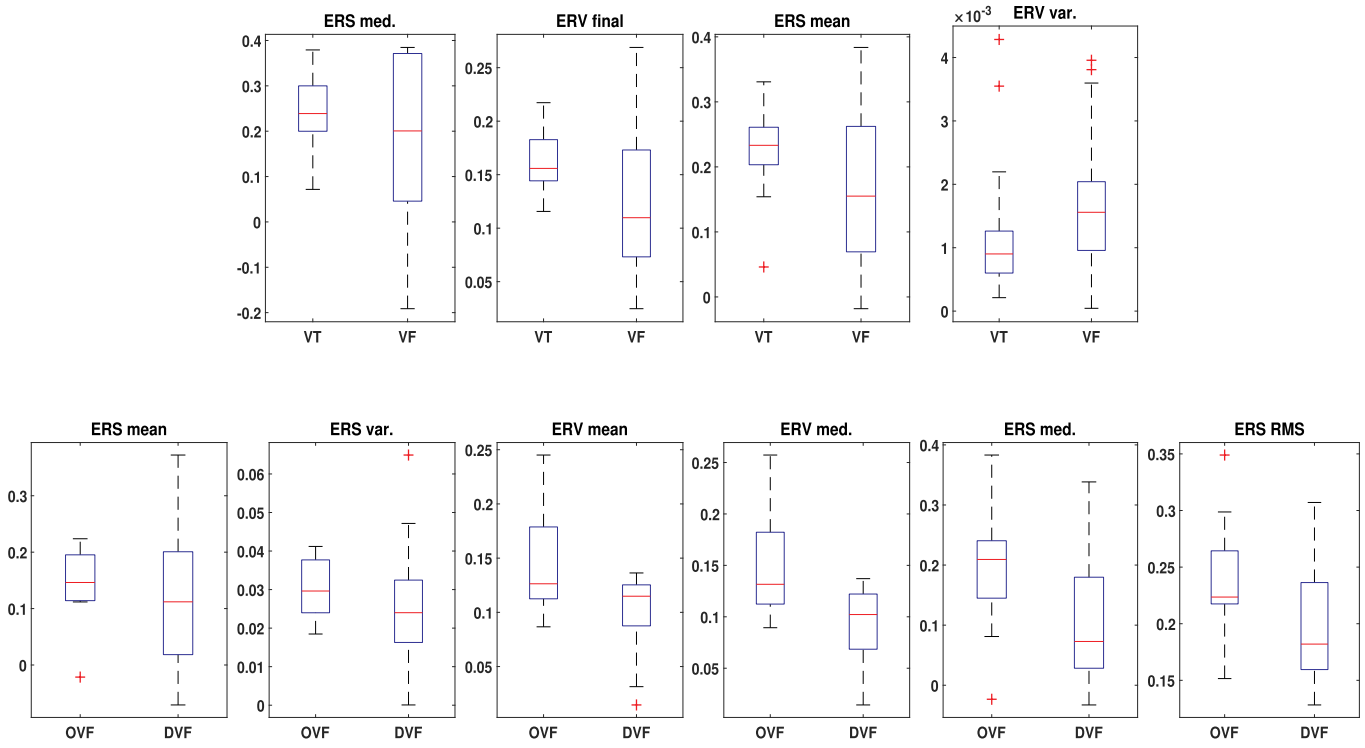

Fig. 4. Boxplots of **Short-Term** features. Top row shows features used for VT vs VF classification and bottom row for OVF vs DVF classification.

feature denoted by the sub-name 'total' was the ERS feature computed over the full 60-s duration of each VA segment. The bottom row of Fig. 5 shows the boxplots of the features used for OVF vs DVF classification. From the bottom row of Fig. 5, it is evident that IE_{12} mean and ERS 'total' are the top 2 dominant features. IE_{12} mean appeared to be generally higher for the OVF group than the DVF group. Since DVF is a worsened state than OVF, this may be reflected in the relative amplitude/energy of the ECG recording. Thus, the mean energy of the top 2 dominant IMFs over time for DVF appeared lower than OVF. The ERS 'total' feature was slightly higher for the OVF group than DVF group. ERS gives an indication of the energy distribution of the IMFs. The OVF group had a slightly higher ERS value because it tends to be more dominated by a few IMFs (less multi-component), while DVF tends to be more multi-component making its ERS less pronounced.

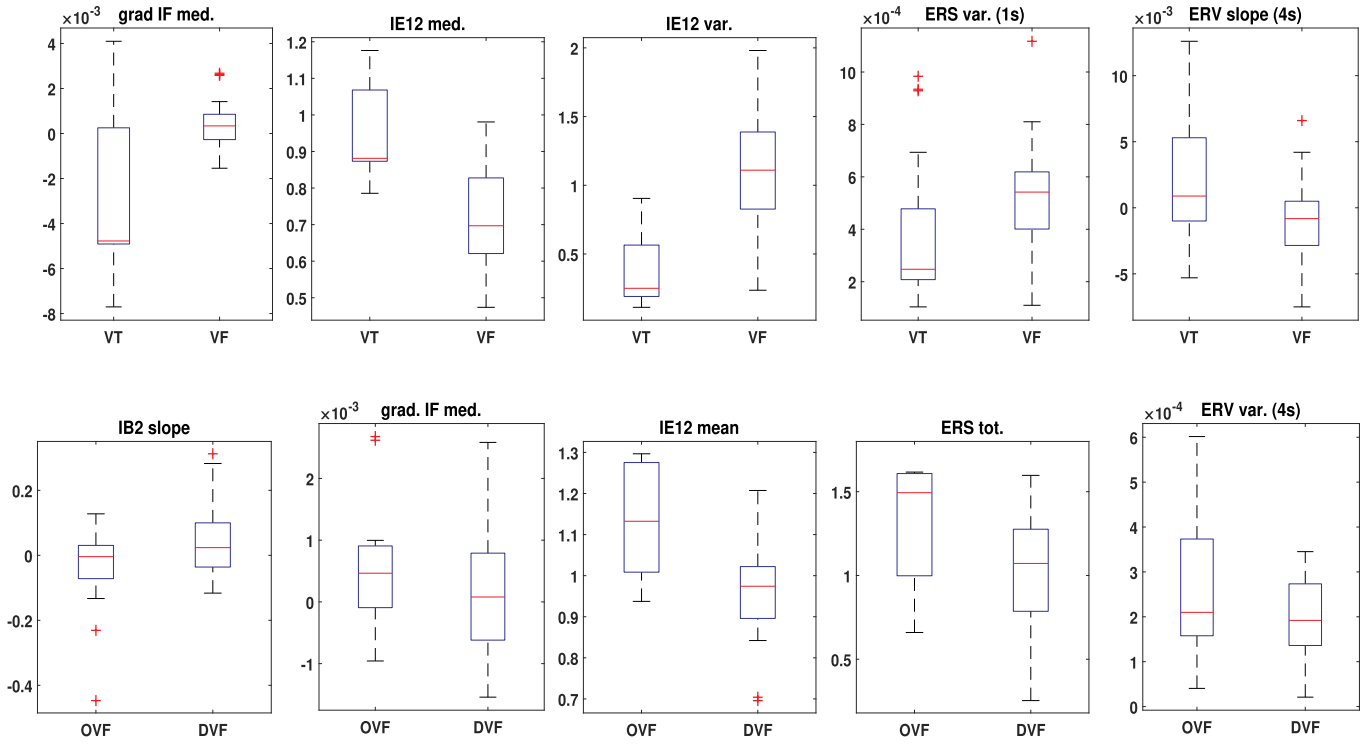

Fig. 5. Boxplots of **Long-Term** features. Top row shows features used for VT vs VF classification and bottom row for OVF vs DVF classification.

Table 2
Classification results of the first stage using LOOCV - VT vs. VF.

Method	Groups	VT	VF	Total
LOOCV	VT	**20**	2	22
	VF	0	**39**	39
%	VT	**90.9**	9.1	100
	VF	0	**100**	100

Table 3
Classification accuracy of the second stage using LOOCV - OVF vs. DVF.

Method	Groups	OVF	DVF	Total
LOOCV	OVF	**15**	2	17
	DVF	3	**19**	22
%	OVF	**88.2**	11.8	100
	DVF	13.6	**86.4**	100

The classification accuracy achieved in Stage II was 87.2%. Assuming that DVF is the true positive class and OVF is the negative class based on relative severity, the sensitivity was 86.4% while the specificity was 88.2%. The classification results are summarized and shown in Table 3. In total, 15 of the 17 OVF segments and 19 of the 22 DVF segments were correctly classified. The AUC for the ROC curve of this classifier was 0.968, which explained the strong classification performance. The overall p-value for the linear discriminant scores (i.e. weighted sum of feature values used for classification) was also significant ($p < 0.01$).

There was no comparative analysis performed for this part of the approach. The DF, EN, and SE features are static features, and require a buffer of data before they can be calculated. Since the comparative features cannot be extracted instantaneously like IF, IB^2 and IE_{12} were, there were no grounds for a fair comparison and was therefore not included. A graphical illustration of binary classifier output is provided in Fig. 6 for both 'out-of-hospital' and 'in-hospital' scenarios.

4.3. VA trend analysis

Shown in Fig. 7 is one DVF sample and its corresponding trend plot below that illustrates the potential value of the trend analysis approach for a real-world emergency situation. In the initial stages of this segment, the VA trend was oscillating between VT and OVF. During the first 15 s, the signal appeared to have relatively stable frequency and minimal amplitude variations, which are characteristic of polymorphic VT (PVT). Then in the subsequent 15 s, the VA trend shifted to OVF due to the increasing level of disorganization within the signal. Afterward, the signal generally trended towards DVF, despite a small deviation towards VT around 45-s mark. The vast change in temporal organization is visible when examining the zoomed-in portions of the signal at the beginning and at towards the end of the segment. The disorganized nature at the end is typical of DVF. This approach provided instantaneous information of the evolution of the VA over time. This near real-time feedback could prove very useful to EMS personnel in 'out-of-hospital' scenarios.

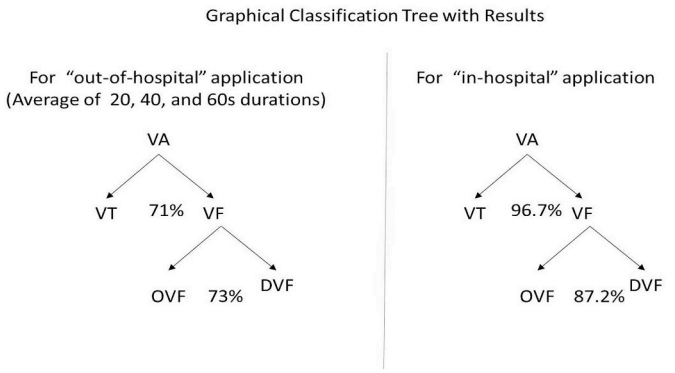

Fig. 6. Graphical illustration of binary classifier output for out-of-hospital and in-hospital scenarios.

In order to verify the VA trend results, an ensemble average of the VA trends for the 3 groups was computed, and the results were shown in the boxplots in Fig. 8. This figure shows that the 3 VA groups separated themselves distinctly when applied to the VA trend approach. The DVF group had the highest average trend score, while OVF had the second highest trend score, and VT had the lowest average trend score. This result corresponded nicely with the VA trend algorithm implemented, in which DVF segments were labeled 2, OVF segments were labeled 1, and VT segments were labeled 0. Overall, this helped to validate the separability of the 3 VA groups using instantaneous features for trend analysis.

5. Discussion

Time critical and informative feedback could assist clinical community to improve the administration of treatment options for VAs. We have presented ECG waveform quantification approaches that enables such a feedback in a timely fashion for 'in-hospital' and 'out-of-hospital' VF scenario. The proposed extraction of instantaneous time-frequency ECG features in a time-efficient manner addresses the requirements for real-time monitoring of VA progression. We have also shown that the proposed long-term dynamic features demonstrate great potential for screening 'in-hospital' patients (and patients with ICDs) for forthcoming VF ablation therapy possibilities. A positive divergence of the proposed approaches compared to traditional approaches is to account for temporal evolution of VA in classifying them rather than labeling them by observing over short windows.

The results for short-term analysis showed that the method became more accurate as the trial durations were increased. The longer the trial duration, the better ERV/ERS windowed features captured the dynamic temporal changes of VAs. Although the classification accuracies of the shorter 20-s and 40-s trials were lower than the 60-s trial, it still gave the user more flexibility as to how and when to utilize the real-time diagnostic feedback. The approach showed fair results, especially for the challenging problem of classifying OVF and DVF in near real-time (i.e. analyzing a 60-s VA in 4s segments in just 0.35s). The results for long-term (in-hospital) VA classification showed through the use of instantaneous and windowed ERV/ERS features, high accuracy can be achieved. Including instantaneous features (IE_{12}, IF, and IB^2) positively influenced the long-term analysis results. The VA trend analysis using instantaneous time-frequency features demonstrated the feasibility of a near real-time monitoring of VAs and the average trend scores agreed with the labeling of the 3 groups.

Considering that the essence of our approaches is to account for temporal evolution of VAs in a computationally efficient manner, performance comparisons with existing works using static features may not be straight forward. However, we discuss a few relevant works with similar motivation of sub-classifying VF. Balasundaram et al. [18] (our previous work) used wavelet-based features to classify VT, OVF, and DVF. The features used previously were tested on this database, and the results were 93.4% for VT vs. VF, and 84.2% for classifying OVF and DVF. The approach proposed in this work performed superior, and most importantly is computationally efficient than Balasundaram et al. Another previous work by Weixin utilized a fuzzy logic approach to discriminate between VT, OVF, and DVF using 10 static ECG features [19]. They reported accuracies of 92.6% for VT vs. VF and 84.5% for OVF vs. DVF classification. They also performed a comparative analysis to Balasundaram et al. and showed slightly better classification results, however, with a larger feature dimension. Tripathy et al. used a variant of EMD called variational mode decomposition to extract simple

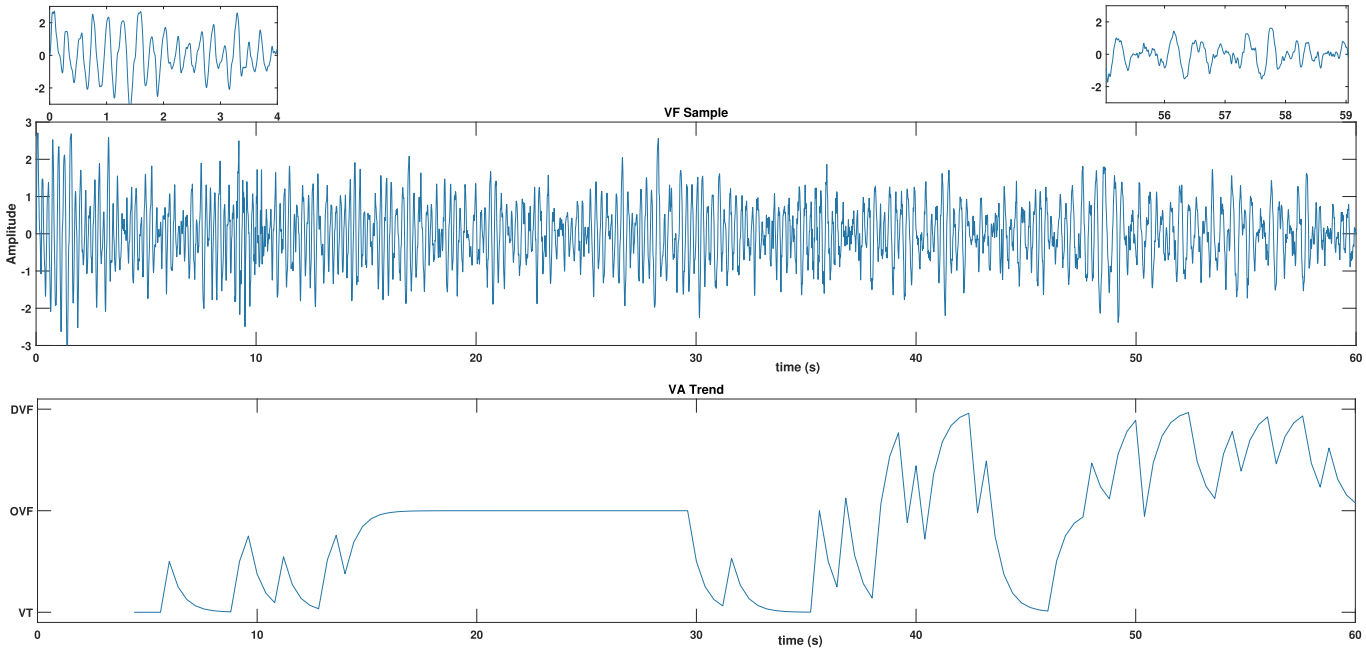

Fig. 7. The plot of a (mostly) DVF sample along with its VA trend signal shown below.

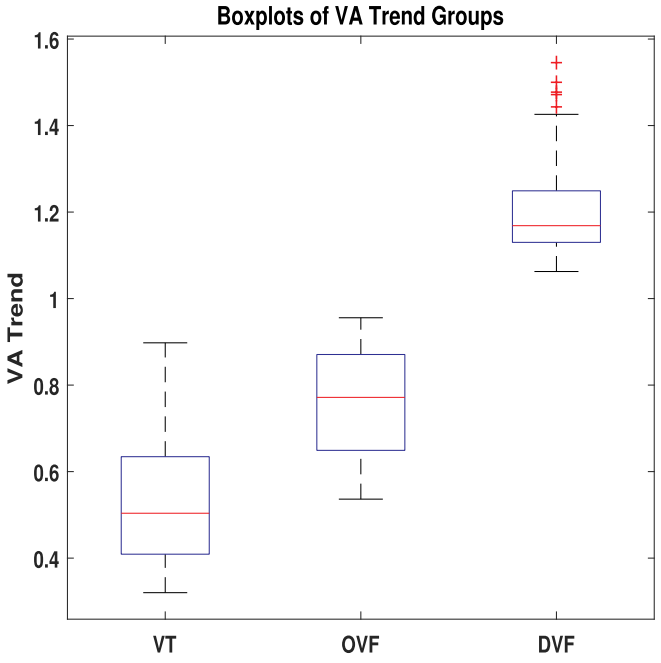

Fig. 8. The boxplots of the ensemble averaged VA trends for the VT, OVF, and DVF groups.

features for separating shockable from non-shockable VAs, achieving a high accuracy of 97% [48]. Although Tripathy's approach was highly accurate, the proposed work tackles the more difficult problem of sub-classifying VF. Joo et al. used artificial neural networks to classify between VT, VF, and 'VT + VF' signals [49]. While their work produced fair results, our work performed considerably better for classifying VT, and it undertook the difficult task of sub-classifying VF effectively.

The proposed approaches for 'out-of-hospital', 'in-hospital', and VA trend analysis can significantly benefit cardiac resuscitation and long-term treatment options. Although the current defibrillators used by EMS and Automatic External Defibrillators (AEDs) are equipped with basic ECG rhythm analysis facilities, proposed short-term feature algorithms can be incorporated in aiding these devices to provide real-time informative feedback on the progression of VAs. VA trend analysis added to such devices in the 'out-of-hospital' VF scenario can provide a visual index in tracking VAs and help choosing appropriate treatment options (i.e. CPR, anti-arrhythmic drugs, defibrillation shock). Using the VA Trend, EMS can visually assess how the patient is responding to the treatment in real-time to see if the treatment is having the intended effect. Other critical use is monitoring the VA Trend to indirectly predict time of VF onset (i.e. longer the time from VF onset, higher probability of DVF) and forewarn EMS to choose appropriate therapy sequence (i.e. CPR first, shock first, anti-arrhythmic drugs etc).The 'in-hospital' techniques using ICD or Holter ECG recordings can provide clinicians with the ability to quantify the trends in VA progression over time and alter treatment options such as ICD programming or screening patients for forthcoming VF ablation strategies.

Each presented approach has its unique strengths and weaknesses. The short-term VA classification approach was able to classify VAs in near real-time with only a 4-s data buffer required, but achieved appreciably lower accuracies than long-term classification. The long-term VA classification approach was able to achieve very high classification accuracies when discriminating VT/VF (96.7%) and OVF/DVF (87%), but since it required 60-s of ECG data to be readily available before it could be used, it is not suitable for use in real-world emergency settings. Lastly, the VA trend analysis is the most capable approach for providing near real-time feedback, since it updates every 100 samples (0.4s) after the initial 4-s buffer. It was useful for evaluating the VA progression over its time duration, rather than providing a direct VA diagnosis. Each of these approaches has its own merits, and should be utilized in applications that accentuate their strengths.

6. Conclusion

This study presented a number of EMD-based approaches useful for optimizing cardiac resuscitation based on EMD. The first approach was a short-term VA classification technique which utilized IMF-energy based features for quantifying temporal organization of VAs over time. This method would prove useful for diagnosing VAs and providing near real-time feedback during 'out-of-hospital' incidents. The second approach was a long-term VA classification technique that demonstrated high accuracy for performing VT/VF and OVF/DVF classification. This

approach was suitable for 'in-hospital' treatment planning and feedback to doctors/clinicians performing retrospective analysis. The third approach was VA Trend Analysis, in which the instantaneous features were used to provide visual feedback on the dynamic evolution of VAs over time. This approach showed potential use in 'out-of-hospital' situations for assisting EMS in selecting and modifying treatment options based on the real-time progression of VAs. The proposed algorithms may be implemented into real-time devices that could be used in the field to help improve VA diagnosis and therapy selection which may hopefully lead to improved patient outcomes. In future studies, additional instantaneous and EMD-based features may be experimented with to improve the classification accuracy of the proposed methods.

7. Limitations

The main limitation of using an EMD-based approach is the issue of mode mixing. It is characterized either by a single IMF containing multiple oscillatory patterns of vastly differing scales (frequencies), or a single scale existing in multiple IMFs [50]. Often the result of signal intermittency, this phenomenon causes the physical interpretation of individual IMFs to be skewed, and may also result in some aliasing in the TF plane of the HS. There are noise-assisted EMD methods that address this problem, but they were computationally prohibitive to the fundamental goals of this work. Noise-assisted EMD methods require epochs of IMF realizations to be generated before the final IMFs are found, making them significantly slower than traditional EMD. Since real-time applications were a focus for this work, keeping the computational cost as low as possible was a priority. Also, although mode mixing disturbs the physical meaning of individual IMFs, the focus of this work was on relative feature extraction between the different VA groups for classification, and not on uncovering mechanistic insights into VF. Thus, mode mixing was not a major concern for this work.

Another potential limitation is the size and scope of the ECG database used in this study. In total, we used 61 60-s ECG VA segments including 39 VF segments. Due to the ethical and practical constraints of acquiring human VF data, it is very difficult to obtain a large VA database, particularly for VF. However, when comparing this database to others used in comparable works, a database of 39 60-s VF segments is still of considerable size and enough to test the validity of the proposed approaches. Also, since the ECG segments used were acquired from publicly available databases, it was not possible to precisely control the duration of the VA segments. Thus, the same 60-s signals were used for multiple approaches in this work, only segmented. Nonetheless, the use of lengthy 60-s VA segments helped to reveal natural variations in the composition of the VAs over time, which enabled for the monitoring and quantification of dynamic VA behaviour.

Conflict of interest statement

None declared.

Acknowledgment

We acknowledge with thanks Natural Sciences and Engineering Research Council of Canada (Grant No. RGPIN-2015-06644) for providing funding support, and contributions from our clinical collaborators at TGH.

References

[1] J.E. Hall, Guyton and Hall Textbook of Medical Physiology, Saunders Elsevier, Philadelphia, PA, 2011.
[2] H.V. Huikuri, A. Castellanos, R.J. Myerburg, Sudden death due to cardiac arrhythmias, N. Engl. J. Med. 345 (20) (2001) 1473–1482.
[3] S. Girotra, S. van Diepen, B.K. Nallamothu, M. Carrel, K. Vellano, M.L. Anderson, B. McNally, B.S. Abella, C. Sasson, P.S. Chan, Regional variation in out-of-hospital cardiac arrest survival in the United States, Circulation 133 (22) (2016) 2159–2168.
[4] D.E. Krummen, J. Hayase, S.P. Vampola, G. Ho, A.A. Schricker, G.G. Lalani, T. Baykaner, T.M. Coe, P. Clopton, W.-J. RAPPEL, et al., Modifying ventricular fibrillation by targeted rotor substrate ablation: proof-of-concept from experimental studies to clinical vf, J. Cardiovasc. Electrophysiol. 26 (10) (2015) 1117–1126.
[5] G. Ho, K.S. Hoffmayer, C.T. Villongco, D. Vidmar, W.-J. Rappel, D.E. Krummen, Successful ventricular fibrillation functional substrate ablation via a single vascular access site, HeartRhythm Case Rep. 4 (5) (2018) 173–176.
[6] D.E. Krummen, J. Hayase, D.J. Morris, J. Ho, M.R. Smetak, P. Clopton, W.-J. Rappel, S.M. Narayan, Rotor stability separates sustained ventricular fibrillation from self-terminating episodes in humans, J. Am. Coll. Cardiol. 63 (24) (2014) 2712–2721.
[7] D.E. Krummen, G. Ho, K.S. Hoffmayer, F. Schweis, A. Bradshaw, T. Baykaner, P.J. Wang, M.N. Viswanathan, W.-J. Rappel, S.M. Narayan, Rotor substrate ablation for antiarrhythmic-refractory ventricular fibrillation with infrequent, multifocal triggers, Circulation 138 (1) (2018) A14 872–A14 872.
[8] R.A. Gray, A.M. Pertsov, J. Jalife, Spatial and temporal organization during cardiac fibrillation, Nature 392 (6671) (1998) 75.
[9] J.F. Huizar, M.D. Warren, A.G. Shvedko, J. Kalifa, J. Moreno, S. Mironov, J. Jalife, A.V. Zaitsev, Three distinct phases of vf during global ischemia in the isolated blood-perfused pig heart, Am. J. Physiol. Heart Circ. Physiol. 293 (3) (2007) H1617–H1628.
[10] S. Masse, E. Downar, V. Chauhan, E. Sevaptsidis, K. Nanthakumar, Ventricular fibrillation in myopathic human hearts: mechanistic insights from in vivo global endocardial and epicardial mapping, Am. J. Physiol. Heart Circ. Physiol. 292 (6) (2007) H2589–H2597.
[11] K. Umapathy, K. Nair, S. Masse, S. Krishnan, J. Rogers, M.P. Nash, K. Nanthakumar, Phase mapping of cardiac fibrillation, Circ. Arrhythmia Electrophysiol. 3 (1) (2010) 105–114.
[12] M.P. Nash, A. Mourad, R.H. Clayton, P.M. Sutton, C.P. Bradley, M. Hayward, D.J. Paterson, P. Taggart, Evidence for multiple mechanisms in human ventricular fibrillation, Circulation 114 (6) (2006) 536–542.
[13] S.V. Pandit, J. Jalife, Rotors and the dynamics of cardiac fibrillation, Circ. Res. 112 (5) (2013) 849–862.
[14] J.J. Menegazzi, C.W. Callaway, L.D. Sherman, D.P. Hostler, H.E. Wang, K.C. Fertig, E.S. Logue, Ventricular fibrillation scaling exponent can guide timing of defibrillation and other therapies, Circulation 109 (7) (2004) 926–931.
[15] Y. Gong, Y. Lu, L. Zhang, H. Zhang, Y. Li, Predict defibrillation outcome using stepping increment of poincare plot for out-of-hospital ventricular fibrillation cardiac arrest, BioMed Res. Int. 2015 (2015).
[16] K. Umapathy, F.H. Foomany, P. Dorian, T. Farid, G. Sivagangabalan, K. Nair, S. Masse, S. Krishnan, K. Nanthakumar, Real-time electrogram analysis for monitoring coronary blood flow during human ventricular fibrillation: implications for cpr, Heart Rhythm 8 (5) (2011) 740–749.
[17] G.A. Ng, Feasibility of selection of antiarrhythmic drug treatment on the basis of arrhythmogenic mechanismrelevance of electrical restitution, wavebreak and rotors, Pharmacol. Ther. vol. 176, (2017) 1–12.
[18] K. Balasundaram, S. Masse, K. Nair, K. Umapathy, A classification scheme for ventricular arrhythmias using wavelets analysis, Med. Biol. Eng. Comput. 51 (1–2) (2013) 153–164.
[19] N. Weixin, A novel algorithm for ventricular arrhythmia classification using a fuzzy logic approach, Australas. Phys. Eng. Sci. Med. 39 (4) (2016) 903–912.
[20] R. Clayton, R. Campbell, A. Murray, "Time-frequency analysis of human polymorphic ventricular tachycardia, In Computers in Cardiology 1997, IEEE, 1997, pp. 97–100.
[21] R. Clayton, A. Murray, "Comparison of techniques for time–frequency analysis of the ecg during human ventricular fibrillation, IEE Proc. Sci. Meas. Technol. 145 (6) (1998) 301–306.
[22] A. Patwardhan, S. Moghe, K. Wang, F. Leonelli, Frequency modulation within electrocardiograms during ventricular fibrillation, Am. J. Physiol. Heart Circ. Physiol. 279 (2) (2000) H825–H835.
[23] S.A. Moghe, Spatio-temporal Variation in Activation Intervals during Ventricular Fibrillation, University of Kentucky, 2002 Doctoral Dissertations.
[24] K. Umapathy, S. Massé, E. Sevaptsidis, J. Asta, S. Krishnan, K. Nanthakumar, Spatiotemporal frequency analysis of ventricular fibrillation in explanted human hearts, IEEE (Inst. Electr. Electron. Eng.) Trans. Biomed. Eng. 56 (2) (2009) 328–335.
[25] N.E. Huang, et al., The empirical mode decomposition and the hilbert spectrum for nonlinear and non-stationary time series analysis, Proc Math Phys Eng Sci, vol. 454, The Royal Society, 1998, pp. 903–995 no. 1971.
[26] N.E. Huang, X. Chen, M.-t. Lo, Z. Wu, On hilbert spectral representation: a true time-frequency representation for nonlinear and nonstationary data, Adv. Adapt. Data Anal. 3 (01n02) (2011) 63–93.
[27] M. Hotradat, K. Balasundaram, S. Masse, K. Nair, K. Nanthakumar, K. Umapathy, Instantaneous time-frequency features in characterizing ventricular arrhythmias using empirical mode decomposition, In 2018 52nd Asilomar Conference on Signals, Systems, and Computers, IEEE, 2018, pp. 1225–1229.
[28] A.L. Goldberger, L.A. Amaral, L. Glass, J.M. Hausdorff, P.C. Ivanov, R.G. Mark, J.E. Mietus, G.B. Moody, C.-K. Peng, H.E. Stanley, Physiobank, physiotoolkit, and physionet: components of a new research resource for complex physiologic signals, Circulation 101 (23) (2000) e215–e220.
[29] H.-U. Strohmenger, K.H. Lindner, C.G. Brown, Analysis of the ventricular fibrillation ecg signal amplitude and frequency parameters as predictors of countershock success in humans, Chest 111 (3) (1997) 584–589.
[30] Y.-H. Wang, C.-H. Yeh, H.-W.V. Young, K. Hu, M.-T. Lo, On the computational complexity of the empirical mode decomposition algorithm, Phys. A Stat. Mech. Appl. 400 (2014) 159–167.

[31] M. Kaleem, et al., Pathological speech signal analysis and classification using empirical mode decomposition, Med. Biol. Eng. Comput. 51 (2013) 811–821.
[32] A. Eftekhar, C. Toumazou, E.M. Drakakis, Empirical mode decomposition: real-time implementation and applications, J. Signal Proces. Syst. 73 (1) (2013) 43–58.
[33] R. Rato, M.D. Ortigueira, A. Batista, On the hht, its problems, and some solutions, Mech. Syst. Signal Process. 22 (6) (2008) 1374–1394.
[34] Z. Wang, Hilbert Transform Applications in Signal Analysis and Non-parametric Identification of Linear and Nonlinear Systems, Doctoral Dissertation Missouri University of Science and Technology, 2011.
[35] K.A. Gladis, K. Ramar, "A novel method for content based image retrieval using the approximation of statistical features, morphological features and bpn network, In Conference on Computational Intelligence and Multimedia Applications, 2007. International Conference on, vol. 3, IEEE, 2007, pp. 179–184.
[36] F. Auger, P. Flandrin, P. Gonçalvès, O. Lemoine, Time-frequency Toolbox vol. 46, *CNRS France-Rice University*, 1996.
[37] P.J. Loughlin, K.L. Davidson, Modified cohen-lee time-frequency distributions and instantaneous bandwidth of multicomponent signals, IEEE Trans. Signal Process. 49 (6) (2001) 1153–1165.
[38] A.O. Andrade, P. Kyberd, S.J. Nasuto, The application of the hilbert spectrum to the analysis of electromyographic signals, Inf. Sci. 178 (9) (2008) 2176–2193.
[39] M.A. Poletti, The development of instantaneous bandwidth via local signal expansion, Signal Process. 31 (3) (1993) 273–281.
[40] T. Soderstrom, H. Fan, B. Carlsson, S. Bigi, Least squares parameter estimation of continuous-time arx models from discrete-time data, IEEE Trans. Autom. Control 42 (5) (1997) 659–673.
[41] M. Malarvili, I. Kamarulafizam, S. Hussain, D. Helmi, Heart sound segmentation algorithm based on instantaneous energy of electrocardiogram, In Computers in Cardiology, 2003, IEEE, 2003, pp. 327–330.
[42] R.O. Duda, P.E. Hart, D.G. Stork, et al., 2nd," *Edition*, Pattern Classification vol. 55, (2001) New York.
[43] IBM Corp, IBM SPSS Statistics for Windows, (2017) version 25.0.
[44] P. Gaur, R.B. Pachori, H. Wang, G. Prasad, An empirical mode decomposition based filtering method for classification of motor-imagery eeg signals for enhancing brain-computer interface, 2015 International Joint Conference on Neural Networks (IJCNN), IEEE, 2015, pp. 1–7.
[45] J.V. Kopke, L.J. Hargrove, M.D. Ellis, Applying lda-based pattern recognition to predict isometric shoulder and elbow torque generation in individuals with chronic stroke with moderate to severe motor impairment, J. NeuroEng. Rehabil. 16 (1) (2019) 35.
[46] S.K. Berkaya, A.K. Uysal, E.S. Gunal, S. Ergin, S. Gunal, M.B. Gulmezoglu, A survey on ecg analysis, Biomed. Signal Process. Control 43 (2018) 216–235.
[47] S.-S. Chang, D. Gunnell, J.A. Sterne, T.-H. Lu, A.T. Cheng, "Was the economic crisis 1997–1998 responsible for rising suicide rates in east/southeast asia? a time–trend analysis for Japan, Hong Kong, South Korea, taiwan, Singapore and Thailand, Soc. Sci. Med. 68 (7) (2009) 1322–1331.
[48] R. Tripathy, L. Sharma, S. Dandapat, Detection of shockable ventricular arrhythmia using variational mode decomposition, J. Med. Syst. 40 (4) (2016) 79.
[49] S. Joo, K.-J. Choi, S.-J. Huh, Prediction of spontaneous ventricular tachyarrhythmia by an artificial neural network using parameters gleaned from short-term heart rate variability, Expert Syst. Appl. 39 (3) (2012) 3862–3866.
[50] Z. Wu, N.E. Huang, Ensemble empirical mode decomposition: a noise-assisted data analysis method, Adv. Adapt. Data Anal. 1 (01) (2009) 1–41.